Iron substitution in CdSe nanoparticles: Magnetic and optical properties

Shashi B. Singh,[1] Mukta V. Limaye,[1] Sadgopal K. Date,[1] Shubha Gokhale,[2,1] and Sulabha K. Kulkarni[3,*]
[1]*DST Unit on Nanoscience, Department of Physics, University of Pune, Pune 411007, India*
[2]*School of Sciences, Indira Gandhi National Open University, New Delhi 110068, India*
[3]*DST Unit on Nanoscience, Indian Institute of Science Education and Research, Pune 411021, India*
(Received 19 May 2009; published 15 December 2009)

Chemically synthesized, thiol capped undoped, and Fe doped CdSe nanoparticles (NPs) have been investigated using a variety of physicochemical techniques. The electron spin resonance spectra exhibit two distinct signals at $g \sim 4$ and $g \sim 2$ characteristic of Fe^{3+} ions occupying highly asymmetric and nearly symmetric lattice sites, respectively. The room temperature Mössbauer studies show a broad asymmetric doublet with isomer shift ~0.35 mm/sec, quadrupole splitting ~0.76 mm/sec characteristic of high spin ferric ions occupying the Cd^{2+} sites with associated changes in local lattice environment. The room temperature photoluminescence spectra show transition from excited state Fe^{3+} ($^4T_1$, $^4T_2$, and ^4E) to the ground-state Fe^{3+} ($^6A_1$) and also suggest that photoexcited electrons are preferentially transferred to iron ion induced trapping centers in CdSe nanoparticles. Room-temperature ferromagnetism is also observed in thiol capped Fe doped CdSe nanoparticles. Significant changes in saturation magnetization value with increasing iron concentration have been observed. The origin of room temperature ferromagnetism and significant change in M_s value are discussed in terms of *F*-center exchange mechanism (bound magnetic polarons).

DOI: 10.1103/PhysRevB.80.235421 PACS number(s): 75.50.Pp, 71.55.Gs, 81.16.Be

I. INTRODUCTION

Electronic materials which can support spin transport at or above room temperature are desired for high performance device applications such as spin field effect transistor, spin light-emitting diode, spin resonant tunneling device, optical switches operating at terahertz frequency, modulators, encoders, decoders, and quantum bits for quantum computation and communication.[1,2] Various materials such as diluted magnetic semiconductors (DMS), half metallic systems, Heusler alloy, etc. are considered to be some of the useful materials in this respect.[2,3] The theoretical work using density functional calculations by Dietl *et al.*[4] have predicted that it is possible to induce room-temperature ferromagnetism (RTFM) in some Mn doped semiconductors such as ZnO and GaN. This work triggered a lot of experimental activity to observe RTFM in a variety of semiconductor thin films.[5] However the subject has become debatable as the origin of ferromagnetism in doped DMS materials was questionable.[5–7] The role of possible extrinsic (magnetic segregation) and/or intrinsic defects in the material is not yet fully understood. Recently, Coey *et al.*[5,8] have discussed the defects (*F* center) induced magnetic exchange as most probable cause of RTFM. It is not yet quite clear whether the F center exchange or any other mechanisms like double exchange or carrier mediated long-range exchange (such as RKKY) play the major role to explain RTFM behavior.[5,8–11]

A new complexity has been added to this issue viz. observation of RTFM in ZnO and gold nanoparticles due to capping molecules.[12,13] Garcia *et al.*[13] showed that thiol capped ZnO nanoparticles showed room temperature ferromagnetic behavior with high saturation magnetization compared to amine and TOPO caped ZnO nanoparticles. Similarly, Crespo *et al.*[12] observed RTFM in thiol capped Au nanoparticles but the gold nanoparticles of the same size when capped with amine molecules exhibited diamagnetism. RTFM and size dependent saturation magnetization tuning is also observed in nitrides,[14] sulphides,[14] and selenides[15] nanoparticles by some groups. Seehra *et al.*[15] reported the occurrence of RTFM in tri-*n*-octylphosphine oxide (TOPO)-tri-*n*-octylphosphine (TOP) capped CdSe nanoparticles and also showed the size as well as temperature effect on the coercivity as well as saturation magnetization. They have attributed the occurrence of ferromagnetism to the presence of *d* holes on the surface of the particles as a result of charge transfer from Cd to TOPO molecules used for the capping. We also reported[16] RTFM in undoped CdSe and Cu doped CdSe nanoparticles. Surface defects were speculated to contribute to RTFM rather than the charge transfer process between surface atoms and the capping molecules. Interestingly another recent report by Meulenberg *et al.*[17] suggests paramagnetic behavior of CdSe nanoparticles, which could be enhanced by variation in end group functionality of the pasivating layer. However, Sundaresan *et al.*[18] propose the universality of RTFM in nanoparticles. Their work on Al_2O_3, CeO_2, SnO_2, In_2O_3, and ZnO nanoparticles without presence of any capping molecules suggests the importance of defects.

Apart from the inherent RTFM of the nanoparticles, it is also important to explore the possibility of tuning the magnetic properties of the nanoparticles. Although size tuning is one option, doping of the nanoparticles is another possibility. However doping of the nanoparticles is usually complicated due to "self-purification" of the nanoparticles.[19] Earlier work[20] on Mn doped ZnS showed that doped Mn preferentially occupies surface sites. Ascertaining the location of the dopant viz. core or surface is rather complex. This is experimentally determined using electron spin resonance (ESR) as there is a difference in the ESR signal for the differently coordinated ions. More over, it is also possible that the crystal structure (local point symmetries) plays an important role in the possibility of doping the nanoparticles. Erwin *et al.*[21] based on the density-functional theory calculations[22] showed that Mn binds preferentially in the zincblende structure

rather than in the wurtzite or rock salt structure. They overcome this problem by making core shell particle in which core is a zincblende seed and a shell of wurtzite material is epitaxially grown to adopt the zincblende structure. They used zincblende ZnSe seeds and epitaxially grew a CdSe shell which could be doped with Mn. Our group[23] also has reported core shell particles of ZnS (zincblende) seed and epitaxially grown Mn doped ZnO shell. Alternatively, it is also possible to optimize the process parameters in the chemical synthesis to obtain desirable crystal structure.[24–26] For example Rogach *et al.*[25] showed the synthesis of CdSe nanoparticles in the zincblende structure. We also are able to get zincblende structure in case of CdSe nanoparticles by low temperature (below 100 °C) chemical route. Other popular chemical synthesis route for high quality CdSe nanoparticles is using TOPO-TOP molecules at high temperature (~300 °C).[27] However, the route produces particles with wurtzite structure. Moreover use of TOPO-TOP as capping molecules as well as organometallic precursors such as dimethylcadmium $[Cd(CH_3)_2]$, which are highly toxic, explosive, expensive in nature, and also the processing parameters and its reproducibility is a matter of great concern.[28] Although, one of the metallo-organic precursor can be replaced with cadmium oxide (CdO) as showed by Peng *et al.*,[28] the toxicity and its processing parameters still remain a drawback of the route. On the other hand, low-temperature synthesis method used here in our work has many advantages such as simple, biocompatible, less toxic, reproducible, and inexpensive chemicals[29,30] compared to TOPO-TOP synthesis route along with the tunability to zincblende structure.

In the present work, we have investigated the effect of iron (Fe) doping concentration on the optical and magnetic properties of CdSe NPs. Interesting changes in the magnetic and optical properties are possible by varying the doping concentration of Fe ions in the CdSe NPs. The samples were characterized by various techniques and discussed in detail in this paper. The observation of RTFM and change in the saturation magnetization (M_s) by changing size of undoped thiol capped CdSe nanoparticles are given in supporting information (S1).[31]

II. EXPERIMENT

A. Synthesis

In order to synthesize undoped and Fe doped CdSe NPs, a simple low-temperature chemical technique[16] was employed with relatively less toxic chemicals as compared to those used in the TOPO-TOP synthesis. In this synthesis route, required amounts of $FeCl_2 \cdot 2H_2O$ (x mmol) and $(CH_3COO)_2Cd.2H_2O$ (2.2-x mmol) were dissolved in 150 mL N, N dimethyl formamide (DMF) to obtain different doping concentrations. Mercaptoethanol was used as a capping agent and added to the above solution, and subsequently, separately prepared solution of sodium selenite in distilled water was drop wise added. The resulting solution was refluxed at 80 °C for 3 h in inert (nitrogen) atmosphere. Acetone was used to precipitate, which was then washed repeatedly by methanol and vacuum dried to obtain nanoparticles.

B. Characterization

Presence of any unintentional (magnetic or otherwise) impurity was checked using x-ray energy dispersive spectrometer (EDS) on JEOL JSM 6360A scanning electron microscope. X-ray diffraction (XRD) investigations of powder samples were performed using Bruker D-8 advance x-ray diffractometer using Cu K_α x-ray source. Transmission electron microscope (TEM) images of the sample were recorded using Tecnai 20 G2 electron microscope operated at 100 kV voltage. Samples for the TEM analysis were prepared by placing a drop of the diluted solution on carbon coated copper grids. Fourier transform infrared (FTIR) of powder samples was performed with a Thermo SCIENTIFIC Nicolet −6700 spectrometer. Photoluminescence (PL) spectra were recorded using a Perkin-Elmer LS-55 spectrofluorometer and the optical absorption spectra were recorded on a Perkin-Elmer Lambda-950 UV-Visible spectrophotometer. The valence-band investigations were carried out using the XUV beamline on INDUS-I storage ring at the Centre for Advanced Technology, Indore, India. 100 eV photon energies were used for the purpose. The photoemission spectra were collected using an Omicron-EA 125 hemispherical analyzer. The spectral resolution was ~200 meV. The samples were prepared in thin film form on silicon substrate. Prior to the measurements, mild Ar^+ ion sputtering was used to remove absorbed species. Electron spin resonance (ESR) spectra of the samples ware recorded using a conventional reflection-type spectrometer (Varian E-112) operating at 9.2 GHz at room temperature (300 K). Room-temperature Mössbauer spectra ($\sim 9 \times 10^7$ counts) were recorded in transmission geometry with a ^{57}Co:Rh source using a commercial spectrometer (Wissel). M-H loops for all the samples carefully packed in the calibrated Teflon sample holder were obtained at the room temperature using vibrating sample magnetometer (VSM) (Lake Shore 7307 model).

III. RESULTS AND DISCUSSION

Figure 1 shows the EDS patterns of CdSe and Fe doped CdSe NPs. It can be noticed that in pure CdSe NPs the peaks due to Cd, Se, S, Si, C, and O are present. There are no magnetic or otherwise impurity peaks present. The Si peak is due to the substrate. S, C, and O peaks are due to the capping molecules (mercaptoethanol) used in the sample synthesis. Presence of unintentional carbon in the vacuum chamber of the SEM may also contribute to the carbon signal. In case of doped CdSe nanoparticles, an additional peak due to Fe is present. The peak intensity increases with increase in Fe concentration in the synthesis. The observed changes in at. wt. % of Cd, Se, and Fe in different samples are shown in the supporting information (S2).[31] By increasing Fe (at. wt. %) concentration, decrease in Cd (at. wt. %) concentration is observed.

The XRD patterns of undoped and Fe doped CdSe NPs with bulk zincblende CdSe (JCPDF 19–0191) peak positions

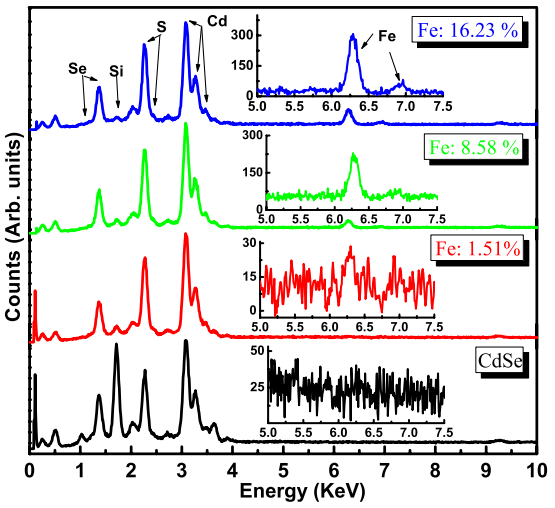

FIG. 1. (Color online) EDS patterns of CdSe and Fe doped CdSe nanoparticles with different Fe (at. wt. 1.51%, 8.58%, and 16.23%) doping percentages. Insets show the enlarged view of EDS patterns in 5–7.5 KeV region.

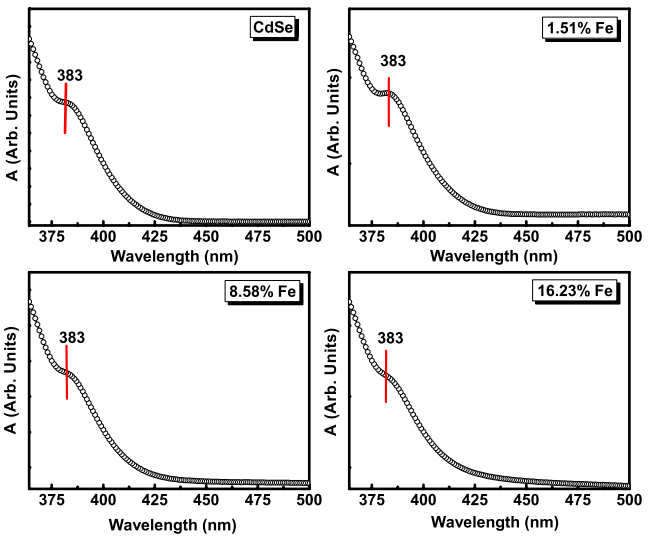

FIG. 3. (Color online) UV-vis absorption spectra for different samples, i.e., pure CdSe NPs, Fe (at. wt. 1.51%) doped CdSe NPs, Fe (at. wt. 8.58 %) doped CdSe NPs, and Fe (at. wt. 16.23%) doped CdSe NPs.

are shown in Fig. 2(a). The broad nature of XRD peaks implies that the particles are of the nanoscale dimension. The average particle size calculated using Scherrer's formula[32]

$$L = \frac{0.9 \times \lambda}{\beta \cos \theta_B},$$

is ~1.9 nm after applying the correction[33] for the spherical particles viz. $D = \frac{4}{3} \times L$. Where L is Scherrer length, λ is wavelength of Cu K_α, β is full width at half maximum, θ_B is the Bragg angle, and D is the particle size. No other crystalline impurity phases are observed for various Fe doped CdSe NPs samples. To find out the size and crystal structure of undoped CdSe NPs we have also performed the TEM [Fig. 2(b)] and selected area electron diffraction studies [Fig. 2(c)]. The particle size determined from the XRD and TEM image match very well. The calculated average particle size from TEM is 2 nm. The electron diffraction pattern implies the zincblende crystalline nature of CdSe NPs.

The absorption spectra of both undoped CdSe and Fe doped CdSe NPs show a peak corresponding to the first excitonic transition ($1s$-$1s$) at ~383 nm (Fig. 3). The particle size calculated using tight binding calculation is $\sim 1.9 \pm 0.1$ nm.[34] Particle sizes can be controlled through changes in the processing parameters. One of them is the

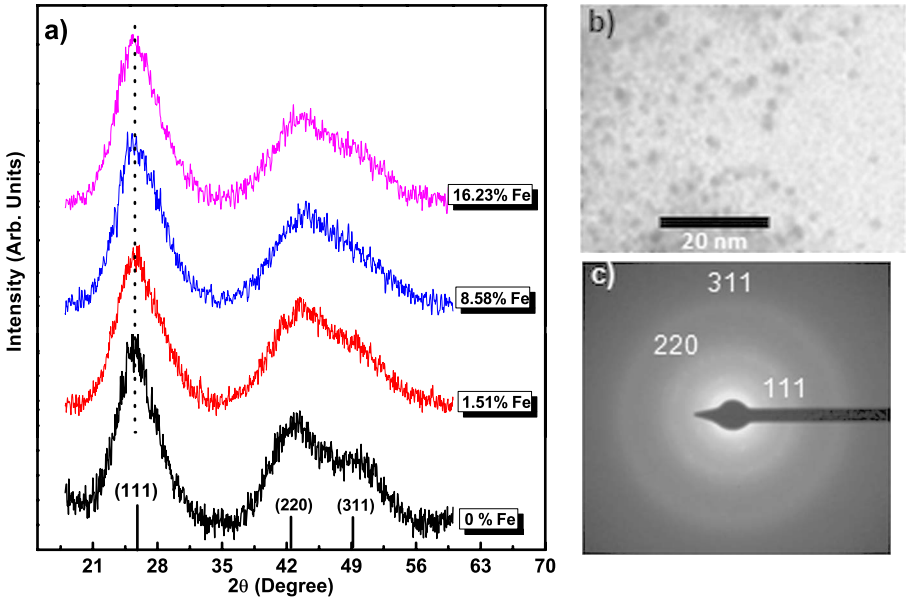

FIG. 2. (Color online) (a) XRD pattern of pure CdSe NPs, Fe (at. wt. 1.51%) doped CdSe NPs, Fe (at. wt. 8.58%) doped CdSe NPs, and Fe (at. wt. 16.23%) doped CdSe NPs with bulk CdSe zincblende peak position. (b) TEM image of pure thiol capped CdSe nanoparticles. (c) Selective area electron diffraction pattern of pure thiol capped CdSe nanoparticles.

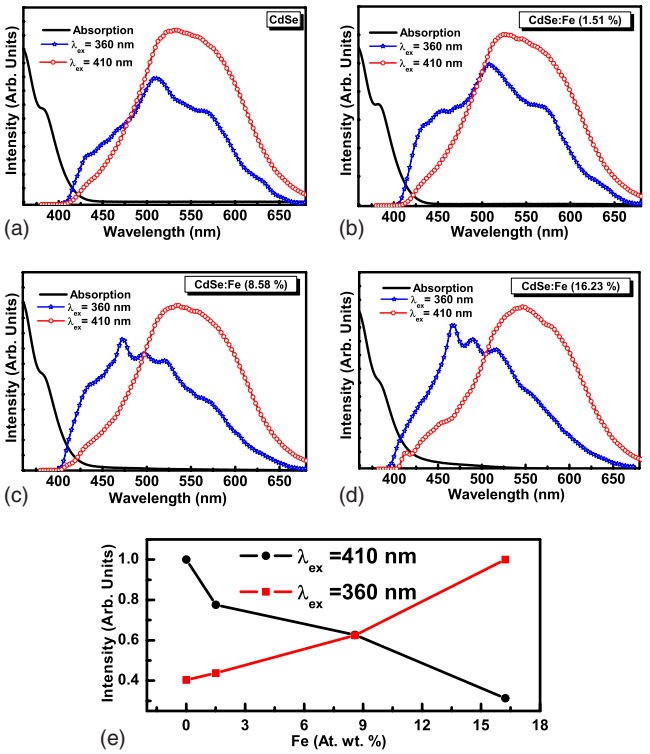

FIG. 4. (Color online) PL Emission spectra (λ_{ex}=360 and 410 nm) with absorption plot of sample (a) pure CdSe NPs, (b) Fe (at. wt. 1.51%) doped CdSe NPs, (c) Fe (at. wt. 8.58%) doped CdSe NPS, and (d) Fe (at. wt. 16.23%) doped CdSe NPs. (e) Plot of emission (λ_{ex}=360 and 410 nm) intensity vs at. wt. % of Fe in CdSe nanoparticles.

concentration of capping molecules in the precursor solutions, providing a tunability of excitonic transition in absorption spectra which are shown in supporting information (S1).[31] The absorption spectra of Fe doped samples show the nearly same peak position with respect to pure CdSe NPs.

In order to understand further the electronic structure of CdSe and Fe doped CdSe NPs, we performed PL analysis shown in Figs. 4(a)–4(d) along with the absorption spectra. The samples were excited with two wavelengths (λ_{ex}=360 and 410 nm). The changes in emission intensity by exciting 360 and 410 nm are shown in Fig. 4(e). Figure 4(a) shows the absorption and emission (λ_{ex}=360 and 410 nm) spectra of pure thiol capped CdSe NPs. The emission spectrum with λ_{ex}= 410 nm shows broad peak at 550 nm. The broad emission is due to excitonic as well as surface defects. The PL peak intensity reduces with increasing doping concentration of iron [Fig. 4(e)]. The iron state acts as an electron trapping center which recombines nonradiatively. This means that photoexcited electrons are preferentially transferred to iron ion induced trapping centers compared to anion defect centers.[35,36] While exciting pure CdSe nanoparticles with higher energy (λ_{ex}=360 nm) the emission spectrum shows some distinct peaks in the rang of 410 to 650 nm. This peak at 432 nm is due to excitonic transition and 510 nm, 569 nm peaks are due to trap level. In case of Fe doped CdSe nanoparticles some new peaks [~473 nm (2.68 eV), ~496 nm (2.50 eV), and ~522 nm (2.38 eV)] start appearing with

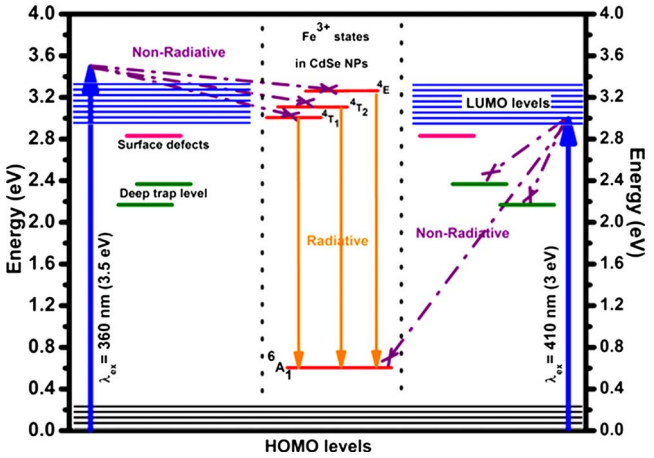

FIG. 5. (Color online) Schematic illustration of the photoluminescence spectroscopic analysis of Fe doped CdSe NPs excited by 410 and 360 nm.

increasing Fe concentration which are not observed in case of 410 nm (3.0 eV) excited spectra. The intensity of this peak increases with increasing iron concentration [Fig. 4(e)]. The appearance of new transition is a clear indication of some new radiative recombination. This new recombination transition at higher energy >2 eV side is possibly due to higher excited state Fe^{3+} ($^4T_1$, $^4T_2$, and ^4E) to the ground state Fe^{3+} ($^6A_1$) transition. Similar transitions were observed by Tanaka *et al.*[37] in case of Mn^{2+} (d^5 configuration) doped ZnS nanoparticles. Such emissive transitions were not observed before in case of Fe doped CdSe nanoparticles at room temperature. These transitions are clear signatures of doping of Fe^{3+} ions in tetrahedral ligand field of wide band gap (3.2 eV) CdSe NPs.

Figure 5 represents the process during the excitation of Fe doped CdSe NPs by 410 nm (3 eV) and 360 nm (3.5 eV), which is similar to the one proposed by Nag *et al.*[38] and Beaulac *et al.*[39] to explain the PL process in case of Mn doped CdS and CdSe quantum dots, respectively. At lower-excitation energy of 3 eV (410 nm) in comparison to 3.5 eV (360 nm), the larger size particles in a given distribution would preferentially be excited. In addition, particles size distribution will result in very closely spaced lowest unoccupied molecular orbital (LUMO) and highest occupied molecular orbital (HOMO) levels. During the excitation process with 3 eV (410 nm), higher $^4T_1$, $^4T_2$, and ^4E states of Fe^{3+} ions are above the LUMO levels and only ground ($^6A_1$) state Fe^{3+} ions are within HOMO-LUMO energy gap and act as electron trapping centers. While exciting with higher energy 3.5 eV (360 nm) all the characteristic states of Fe^{3+} ions ($^4T_1$, $^4T_2$, ^4E, and $^6A_1$) are within LUMO levels and recombine radiatively.

To understand the electronic structure of the doped and undpoed samples, valence-band measurements were carried out using photoemission spectroscopy. Figure 6 shows the valence-band spectra for pure CdSe, 1.51%, and 16.23% Fe doped CdSe nanoparticles, investigated with 100 eV photon energy. This higher photon energy was preferred since the Fe 3*d* emission is known to become more dominant at higher energies.[40] Pure CdSe nanoparticles spectrum exhibits the

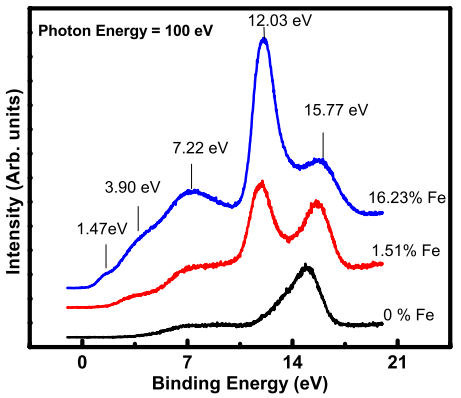

FIG. 6. (Color online) Valence-band spectra of undoped and Fe doped CdSe nanoparticles with 100 eV photon energy.

valence band maximum (VBM) at 3.88 eV and has considerably low density of states characteristic of its semiconductor nature. Three peaks at 3.47, 5.39, and 11.04eV below VBM are evident. The peak at 11.04eV is attributed to Cd 4*d* emission. All these features are shifted to higher binding energy values as compared to bulk CdSe spectra and are in agreement with the earlier report of enhancement in binding energy with decrease in the particle size.[41] With the doping of iron (at. wt. 1.51% and 16.23%) in CdSe nanoparticles the valence band exhibits enhanced density of states near the Fermi level with distinct features at 1.47, 3.90, and 7.22 eV, which increase in the intensity with increasing iron content. These compare well with the valence band of Fe_2O_3, when the contribution of oxygen is removed from the spectrum.[42,43] Hence these could be attributed to the Fe^{3+} state of iron, supporting the results obtained from the PL investigations.

The ESR spectra of pure CdSe nanoparticles and different concentrations of Fe doped CdSe NPs are shown in Fig. 7(a). Figure 7(b) shows the "*g*" values corresponding to different Fe atomic weight percentages in CdSe NPs. CdSe, in its bulk form is a diamagnetic material[15] having magnetic susceptibility -2.25×10^{-7} emu g^{-1} Oe^{-1}. It shows a broad but definite paramagnetic resonance peak centered at $g\sim2.0$ in the NPs. The origin of ESR peak can be due to the presence of

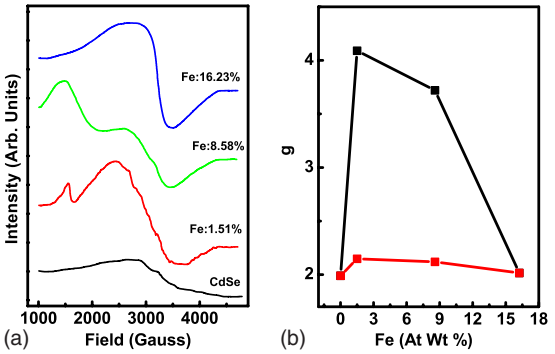

FIG. 7. (Color online) (a) ESR spectra of pure CdSe and different concentration of Fe (at. wt. 1.52%, 8.58%, and 16.23%) doped CdSe nanoparticles. (b) Fe (at. wt. %) vs *g* plot of Fe doped CdSe nanoparticles.

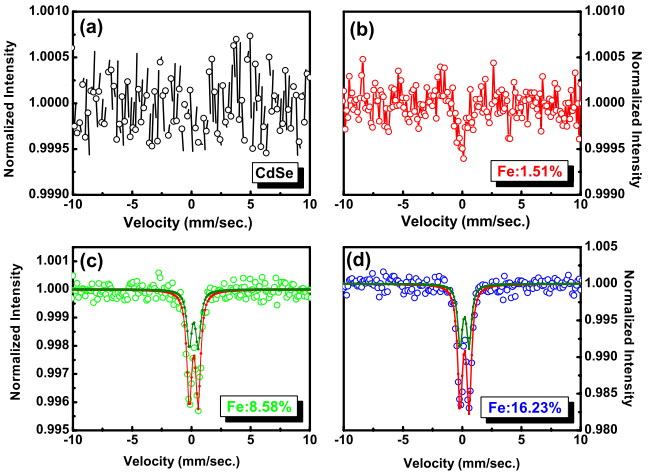

FIG. 8. (Color online) Mössbauer spectra of (a) pure CdSe NPs, (b) Fe (at. wt. 1.51%) doped CdSe NPs, (c) Fe (at. wt. 8.58%) doped CdSe NPs, and (d) Fe (at. wt. 16.23%) doped CdSe NPs.

paramagnetic (capping molecules) species or defects in the sample. The doped samples have $g\sim2.15$ (Fe 1.51%), $g\sim2.12$ (Fe 8.58%), and $g\sim2.01$ (Fe 16.23%). Additionally we observe a relatively sharp peak with a large g value of ~4.2 for Fe (1.51%) sample and broad peak with large g value of ~3.7 for Fe (8.58%) sample. Based on the well accepted spin-Hamiltonian formalism,[44,45] the sharp line at $g\sim4.2$ can be assigned to the isolated Fe^{3+} ions in a distorted local symmetry of surrounding selenium ions and further, these Fe^{3+} ions are isolated with very weak exchange interaction. Additional broad peak at $g\sim2.1$ can be assigned to strongly interacting ferric ions occupying the substitutional lattice position with no local distortion.[44,45] Similar room temperature ESR spectra were recently observed by Singhal *et al.*[46] in case of iron doped indium oxide nanoparticles.

To probe the local lattice environment prevailing around the Fe sites and also to determine the oxidation state and the local lattice symmetry of Fe ions in the CdSe NPs, we have employed Fe^{57} Mössbauer spectroscopy technique. Figures 8(a)–8(d) shows the Mössbauer spectra of pure CdSe sample (~2 nm) and iron doped (1.51%, 8.58%, and 16.23%) samples at room temperature. Absence of any clear absorption peak in the CdSe sample [Fig. 8(a)] indicates that Fe concentration in the sample is less than the detection limit. In case of 1.51% Fe doped sample [Fig. 8(b)] very weak absorption appears. The Mössbauer studies of Fe doped 8.58% and 16.23% sample show [Figs. 8(c) and 8(d), respectively] a broad asymmetric doublet with isomer shift 0.35 and 0.36 mm/sec and quadrupole splitting 0.75 and 0.77 mm/sec, respectively, characteristic of high spin ferric (Fe^{3+}) ions.[11,46] The non-Lorentzian line shape in Mössbauer spectra at room temperature is a well-defined signature of electron spin-spin interactions between iron ions. Due to the broadened and non-Lorentzian line shape, we have not attempted to fit the Mössbauer spectra into two subspectra corresponding to two different sites occupied by iron ions in CdSe NPs. Additional experiments at low temperature are in progress.

Magnetic measurements of the samples are illustrated in Fig. 9. A distinct hysteresis behavior has been observed for

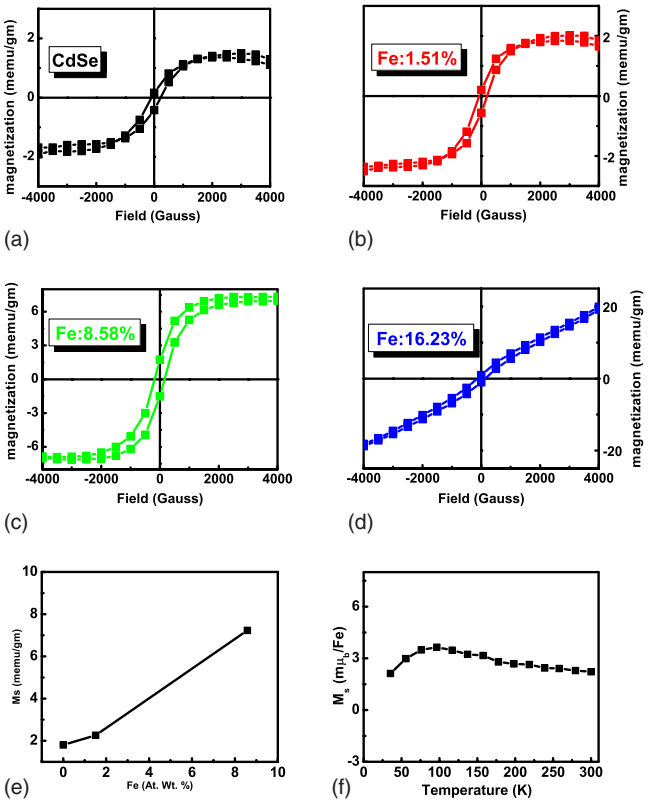

FIG. 9. (Color online) Room temperature (300 K) magnetization curve after background correction (a) CdSe nanoparticles, (b) Fe (at. wt. 1.51%) doped CdSe nanoparticles, (c) Fe (at. wt. 8.58%) doped CdSe nanoparticles, and (d) Fe (at. wt. 16.23%) doped CdSe nanoparticles. (e) Plot of saturation magnetization vs Fe (at. wt.) doping percentage in CdSe nanoparticles. (f) Magnetization vs temperature curve for 8.58% Fe doped CdSe nanoparticles in the ZFC conditions for the applied field value 1000 Oe.

CdSe NPs. For pure CdSe NPs sample the saturation magnetization is ~1.8 memu/gm and the coercivity is ~157 G at room temperature. Although these values are smaller than M_s and H_c values of CdSe NPs reported earlier,[16] it should be noted that the values are strongly dependent on the size of the particles and shown in supporting information (S1).[31] Interestingly here it fits very well with the profound idea of the origin of ferromagnetism is the presence of surface defects and capping molecules.[12–18] With 1.51% doping the M_s increases to ~2.26 memu/gm [Fig. 9(b)] and for 8.58% Fe doped CdSe NPs the M_s is ~7.23 memu/gm [Fig. 9(c)]. The increase in M_s value in comparison to those in the undoped CdSe NPs is due to iron concentration. With further increase in Fe (16.23%) concentration [Fig. 9(d)] the iron-iron magnetic exchange dominates. The changes in saturation magnetization with respect to Fe doping percentage are shown in Fig. 9(e). Magnetization (μ_b/Fe atom) versus temperature curve for 8.58% Fe doped CdSe NPs in the zero-field cooled (ZFC) condition for the applied field value 1000 Oe is shown in Fig. 9(f). It indicates that the ferromagnetic to paramagnetic transition temperature is well above room temperature.

All our experimental results indicate the incorporation of Fe^{3+} ions in different sites in CdSe NPs. Here ferric ions are

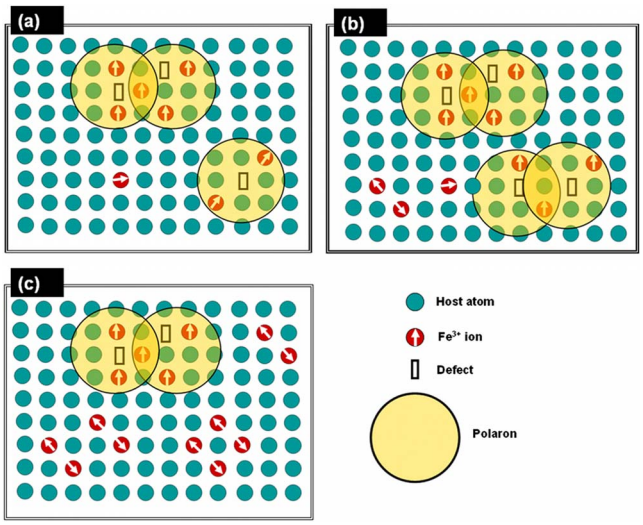

FIG. 10. (Color online) (a) Fe (at. wt. 1.51%) doped CdSe NPs, (b) Fe (at. wt. 8.58%) doped CdSe NPS, and (c) Fe (at. wt. 16.23%) doped CdSe NPs.

strongly coupled in the increasing iron concentration. Therefore, an *F*-center exchange (FCE) mechanism proposed by Coey *et al.*[5,8] in the case of Fe doped SnO_2 thin films have been used to explain the ferromagnetism in Fe doped CdSe nanocrystals. Such (FCE) mechanism expects that an electron trapped in the vacancy makes an *F* center, where the electron occupies an extended orbital which overlaps the *d* shells of both iron neighbors. The exchange interaction between two irons via *F* center leads to the ferromagnetic coupling, where *F* center is similar to bound magnetic polaron. Usually, if Fe occupies substitutional site in a defect-free CdSe crystal, the charge state of iron ion will be +2. Both EPR and Mössbauer results confirm the presence of Fe^{3+} ions within the sample. The charge imbalance between Cd^{2+} and Fe^{3+} ions produces more number of defects within the CdSe NPs and electrons are trapped in defects (*F* center). These defects are further getting modified due to capping molecules. The number of *F* centers and interaction between two iron ions via these *F* centers is highly dependent on Fe concentration. Figure 10 illustrates the overall picture of the observed ferromagnetism at different concentrations of Fe doped CdSe nanoparticles. It is clear from Fig. 10(a) and 10(b) that as Fe concentration increases there is an increase in the *F* centers or bound magnetic polarons. In case of heavily (16.23%) Fe doped CdSe nanoparticles [Fig. 10(c)] the antiferromagnetic (Fe^{3+}-Se^{2+}-Fe^{3+}) exchange interaction between iron ions dominates the ferromagnetic interaction.[5,8] The strong exchange interaction of iron ions is also observed in ESR ($g \sim 2$). The observation of room temperature ferromagnetism in pure thiol capped CdSe nanoparticles is due to combined effect of surface defects and modification due to capping molecules. The change in saturation magnetization with respect to the particle size (thiol capped CdSe nanoparticles) is shown in supporting information (S1),[31] and will be discussed elsewhere.

IV. CONCLUSION

We have successfully doped CdSe NPs with iron (Fe^{3+}) ions. The photoluminescence suggest the doping of Fe^{3+} ions in cubic ligand field of CdSe NPs. The ESR, Mössbauer, and valence band spectra confirm that the iron ions occupy highly asymmetric and nearly symmetric lattice sites with Fe^{3+} ions. These Fe^{3+} ions produce large number of *F* centers due to charge imbalance between Cd^{2+} ions and Fe^{3+} ions. The origin of RTFM and significant change in M_s value are discussed in terms of *F* center exchange mechanism (bound magnetic polarons).

ACKNOWLEDGMENTS

This work was supported by BRNS and DST India. S.K.K. thanks UGC India, for financial support. S.B.S. thanks CSIR India, for financial support. M.V.L. thanks BRNS, India, for financial support. The authors thank UGC-DAE Consortium for the Scientific Research, Indore and D. M. Phase for photoemission investigations. The authors would also like to thank SAIF, IIT Bombay, Mumbai for their help in ESR measurements.

*s.kulkarni@iiserpune.ac.in

[1] S. A. Wolf, D. D. Awschalom, R. A. Buhrman, J. M. Daughton, S. von Molnar, M. L. Roukes, A. Y. Chtchelkanova, and D. M. Treger, Science **294**, 1488 (2001).
[2] I. Žutić, J. Fabian, and S. Das Sarma, Rev. Mod. Phys. **76**, 323 (2004).
[3] S. A. Chambers and Y. K. Yoo, MRS Bull. **28**, 706 (2003).
[4] T. Dietl, H. Ohno, F. Matsukura, J. Cibert, and D. Ferrand, Science **287**, 1019 (2000).
[5] J. M. D. Coey, M. Venkatesan, and C. B. Fitzgerald, Nature Mater. **4**, 173 (2005).
[6] A. Tiwari, M. Snure, D. Kumar, and J. T. Abiade, Appl. Phys. Lett. **92**, 062509 (2008).
[7] A. H. MacDonald, P. Schiffer, and N. Samarth, Nature Mater. **4**, 195 (2005).
[8] J. M. D. Coey, A. P. Douvalis, C. B. Fitzgerald, and M. Venkatesan, Appl. Phys. Lett. **84**, 1332 (2004).
[9] T. Dietl and H. Ohno, MRS Bull. **28**, 714 (2003).
[10] S. A. Chambers, T. C. Droubay, C. M. Wang, K. M. Rosso, S. M. Heald, D. A. Schwartz, K. R. Kittilstved, and D. R. Gamelin, Mater. Today **9**, 28 (2006).
[11] D. Karmakar, S. K. Mandal, R. M. Kadam, P. L. Paulose, A. K. Rajarajan, T. K. Nath, A. K. Das, I. Dasgupta, and G. P. Das, Phys. Rev. B **75**, 144404 (2007).
[12] P. Crespo, R. Litrán, T. C. Rojas, M. Multigner, J. M. de la Fuente, J. C. Sánchez-Lóper, M. A. García, A. Hernando, S. Penadés, and A. Fernández, Phys. Rev. Lett. **93**, 087204 (2004).
[13] M. A. Garcia, J. M. Merino, E. F. Pinel, A. Quesada, J. D. L. Venta, M. L. R. Gonzalez, G. R. Castro, P. Crespo, J. Llopis, J. M. Gonzalez-Calbet, and A. Hernando, Nano Lett. **7**, 1489 (2007).
[14] C. Madhu, A. Sundaresan, and C. N. R. Rao, Phys. Rev. B **77**, 201306(R) (2008).
[15] M. S. Seehra, P. Dutta, S. Neeleshwar, Y.-Y. Chen, C. L. Chen, S. W. Chou, C. C. Chen, C.-L. Dong, and C.-L. Chang, Adv. Mater. **20**, 1656 (2008).
[16] S. B. Singh, M. V. Limaye, S. K. Date, and S. K. Kulkarni, Chem. Phys. Lett. **464**, 208 (2008).
[17] R. W. Meulenberg, J. R. I. Lee, S. K. McCall, K. M. Hanif, D. Haskel, J. C. Lang, L. J. Terminello, and T. van Buuren, J. Am. Chem. Soc. **131**, 6888 (2009).
[18] A. Sundaresan, R. Bhargavi, N. Rangarajan, U. Siddesh, and C. N. R. Rao, Phys. Rev. B **74**, 161306(R) (2006).
[19] G. M. Dalpian and J. R. Chelikowsky, Phys. Rev. Lett. **96**, 226802 (2006).
[20] P. H. Borse, D. Shrinivas, R. F. Shinde, S. K. Date, W. Vogel, and S. K. Kulkarni, Phys. Rev. B **60**, 8659 (1999).
[21] S. C. Erwin, L. J. Zu, M. I. Haftel, A. L. Efros, T. A. Kennedy, and D. J. Norris, Nature (London) **436**, 91 (2005).
[22] G. Kresse and J. Furthmuller, Phys. Rev. B **54**, 11169 (1996).
[23] M. V. Limaye, S. B. Singh, S. K. Date, R. S. Gholap, and S. K. Kulkarni, Mater. Res. Bull. **44**, 339 (2009).
[24] W.-C. Kwak, Y.-M. Sunga, T. G. Kim, and W.-S. Chae, Appl. Phys. Lett. **90**, 173111 (2007).
[25] A. L. Rogach, A. Kornowski, M. Gao, A. Eychmüller, and H. Weller, J. Phys. Chem. B **103**, 3065 (1999).
[26] X. Chen, J. L. Hutchison, P. J. Dobson, and G. Wakefield, J. Mater. Sci. **44**, 285 (2009).
[27] C. B. Murray, D. J. Norris, and M. G. Bawendi, J. Am. Chem. Soc. **115**, 8706 (1993).
[28] Z. A. Peng and X. Peng, J. Am. Chem. Soc. **123**, 183 (2001).
[29] N. Gaponik, D. V. Talapin, A. L. Rogach, K. Hoppe, E. V. Shevchenko, A. Kornowski, A. Eychmuller, and H. Weller, J. Phys. Chem. B **106**, 7177 (2002).
[30] Y. Liu, W. Chen, A. G. Joly, Y. Wang, C. Pope, Y. Zhang, J.-O. Bovin, and P. Sherwood, J. Phys. Chem. B **110**, 16992 (2006).
[31] See EPAPS Document No. E-PRBMDO-80-005947 for supporting text and figures. For more information on EPAPS, see http://www.aip.org/pubservs/epaps.html.
[32] A. Guinier, *X-Ray Diffraction* (Freeman, San Francisco, 1963).
[33] M. G. Bawendi, A. R. Kortan, M. L. Steigerwald, and L. E. Brus, J. Chem. Phys. **91**, 7282 (1989).
[34] S. Sapra and D. D. Sarma, Phys. Rev. B **69**, 125304 (2004).
[35] M. Homyonfer, H.-H. Strehblow, W. Giriat, and R. Tenne, Phys. Rev. B **47**, 1244 (1993).
[36] P. H. Borse, N. Deshmukh, R. F. Shinde, S. K. Date, and S. K. Kulkarni, J. Mater. Sci. **34**, 6087 (1999).
[37] M. Tanaka, J. Qi and Y. Masumoto, J. Lumin. **87-89**, 472 (2000).
[38] A. Nag, S. Sapra, C. Nagamani, A. Sharma, N. Pradhan, S. V. Bhat, and D. D. Sarma, Chem. Mater. **19**, 3252 (2007).
[39] R. Beaulac, P. I. Archer, S. T. Ochsenbein, and D. R. Gamelin, Adv. Funct. Mater. **18**, 3873 (2008).
[40] A. Fujimori, M. Saeki, N. Kimizuka, M. Taniguchi, and S. Suga, Phys. Rev. B **34**, 7318 (1986).
[41] P.-J. Wu, K.-D. Tsuei, K.-H. Weid, and K. S. Liang, Solid State Commun. **141**, 6 (2007).
[42] I. D. Welsh and A. M. A. Sherwood, Phys. Rev. B **40**, 6386

(1989).
[43] A. Fujimori, N. Kimizuka, M. Taniguchi, and S. Suga, Phys. Rev. B **36**, 6691 (1987).
[44] M. Jiang, J. Terra, A. M. Rossi, M. A. Morales, S. E. M. Baggio, and D. E. Ellis, Phys. Rev. B **66**, 224107 (2002).
[45] T. J. Castner, G. S. Newell, W. C. Holton, and C. P. Slichter, J. Chem. Phys. **32**, 668 (1960).
[46] A. Singhal, S. N. Achary, J. Manjanna, O. D. Jayakumar, R. M. Kadam, and A. K. Tyagi, J. Phys. Chem. C **113**, 3600 (2009).